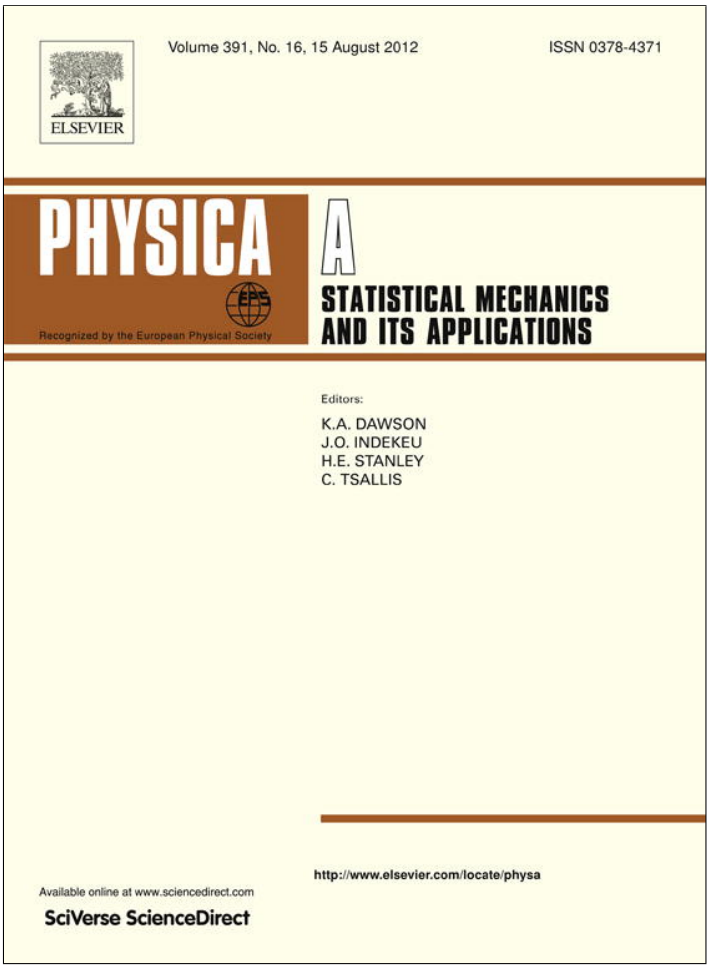

Physica A 391 (2012) 4070–4080

Contents lists available at SciVerse ScienceDirect

Physica A

journal homepage: www.elsevier.com/locate/physa

Formation and synchronization of autocatalytic noise-sustained structures under Poiseuille flow

Alejandro D. Sánchez [1], Gonzalo G. Izús [1], Roberto R. Deza *

Laboratorio de Sistemas Complejos, Instituto de Investigaciones Físicas de Mar del Plata (IFIMAR, UNMdP–CONICET), Deán Funes 3350, B7602AYL Mar del Plata, Argentina

ARTICLE INFO

Article history:
Received 27 November 2011
Available online 28 January 2012

Keywords:
DIFICI
NSS
Gray–Scott
Synchronization
Stability

ABSTRACT

The formation and synchronization of 2D noise-sustained structures are investigated for Gray–Scott kinetics in packed-bed reactors under Poiseuille flows, when identical systems are submitted to independent spatiotemporal Gaussian white noise sources. A finite-wavelength instability is theoretically predicted and numerically confirmed for uncoupled reactors. In particular, noise-sustained structures that flow with viscous boundary conditions are numerically observed above threshold. When the systems are coupled in master–slave configuration, the numerical simulations show that the slave system replicates to a very high degree of precision the convective patterns arising in the master one due to the selective amplification of noise. The nature of the synchronization and the stability of the synchronization manifold are elucidated.

1. Introduction

Synchronization phenomena have been a topic of scientific research for many years [1,2] and in many systems, ranging from physics to biology [3], being ubiquitous in almost every scientific discipline. Since the most recent accounts on the status of this active field of pure and applied research [4–9] it has continued to grow at an explosive rate, incorporating new problems and perspectives, especially with regard to the synchronization of complex networks [10–12]. Many different situations have been considered, including synchronization of limit cycle oscillators [13–15], synchronization of chaotic systems [16], partial (i.e. phase) synchronization [17], generalized synchronization [18,19], synchronization of stochastic systems [20], etc. These works refer mainly to systems characterized by a purely temporal dynamics. A less explored field is the synchronization between continuous systems [21–25], in particular the synchronization of spatiotemporally chaotic fields [26–28] or stochastic fields [29–33].

In this paper we shall restrict our scope to non-delayed synchronization between stochastic fields. In particular, a topic that has been hardly addressed is the synchronization between noise-sustained structures (NSS) in systems undergoing a convective instability [32–34].

A convectively unstable regime is characterized by the fact that local perturbations to the steady state are advected more rapidly than their spreading rate [35–37]. When seen in a Lagrangian framework, the system is unstable; but from a Eulerian description – however – perturbations are "washed out by the flow". Macroscopic patterns named noise sustained structures (NSS) emerge in this regime if noise is present at all times. It is through dynamical amplification of random fluctuations that the system is driven out of its linearly unstable steady state towards the state sustaining NSS. Thus, if noise (or any external deterministic forcing) were not present, nonequilibrium structures could not arise. In fluid

* Corresponding author. Tel.: +54 2234953439; fax: +54 2234753150.
E-mail addresses: sanchez@mdp.edu.ar (A.D. Sánchez), izus@mdp.edu.ar (G.G. Izús), deza@mdp.edu.ar, rrdezab@gmail.com (R.R. Deza).
[1] Member of CONICET, Argentina.

0378-4371/$ – see front matter © 2012 Published by Elsevier B.V.
doi:10.1016/j.physa.2012.01.016

dynamics, for example, the NSS are a spatial macroscopic manifestation of amplified thermal fluctuations. NSS have been observed in fluid convection experiments (both in open flow configuration [38] and Taylor–Couette flows [39,40]), and their precursors have been also observed in nematic liquid crystals [41]. They have also been numerically shown to exist in optical systems [32,33,42–44] (driven in this case by quantum noise) and in an autocatalytic chemical reaction – the Gray–Scott (GS) model – taking place in a differential-flow reactor [45].

In previous works [34,45,46] we have investigated the synchronization of NSS for a cubic stochastic kinetics in extended chemical reactors, linearly coupled and submitted to a uniform external flow. The theoretical analysis reveals the existence of synchronization between the stochastic fields, but the results are restricted to the idealized situation of an unrealistic uniform flow. In this paper we extend that analysis to investigate the phenomena of pattern formation and synchronization of nonequilibrium structures for stochastic cubic kinetics, in extended reactors submitted to Poiseuille flow, i.e., under viscous boundary conditions that affect the shape and propagation of the resulting structures.

The paper is organized as follows: Section 2 reviews the equations for the isolated GS system under Poiseuille flow. The linear stability analysis of the steady state solution and the features of the resulting patterns are also discussed here. In Section 3 we illustrate the replication of NSS under unidirectional coupling and we characterize the stability of the synchronized manifold in terms of damped dynamics of Fourier modes. Finally, we summarize the main conclusions in Section 4.

2. Noise-sustained structures

2.1. The Gray–Scott kinetics

The GS model describes a three-step reaction, with the intermediate one having cubic autocatalytic kinetics:

$$P \xrightarrow{k_0} A$$
$$A + 2B \xrightarrow{k_1} 3B$$
$$B \xrightarrow{k_2} C.$$

In our case, the reaction is assumed to take place in a two-dimensional, differential-flow and packed-bed reactor, where A is immobilized while B is free to diffuse and is also advected by a flow. Moreover, the reaction is maintained out of equilibrium by keeping the concentration of the precursor species P constant ($p = p_0$) and that of the inert product C zero ($c = 0$), i.e. it is immediately removed from the reactor.

After scaling concentrations by $(k_2/k_1)^{1/2}$, time by k_2^{-1} and length by $(D_B/k_2)^{1/2}$, the rate equations for the system read

$$\partial_t a_1 = \mu - a_1 b_1^2 + \xi_1(\vec{r}, t),$$
$$\partial_t b_1 = \nabla^2 b_1 - \vec{\phi}.\vec{\nabla} b_1 - b_1 + a_1 b_1^2, \tag{1}$$

where $a_1(\vec{r}, t)$ and $b_1(\vec{r}, t)$ are the local concentrations of A and B, respectively. μ stands for the scaled version of $k_0 p_0$ and the vector field $\vec{\phi}$ is that of a Poiseuille flow parallel to the longitudinal reactor axis (x direction), whose expression is

$$\vec{\phi}(\vec{r}) = \phi(y)\hat{x} = \frac{3}{2}\phi_m\left(1 - 4\frac{y^2}{L_y^2}\right)\hat{x}. \tag{2}$$

Here ϕ_m is the average fluid flux, and the flow velocity vanishes at the reactor walls $y = \pm L_y/2$ due to viscosity. Finally, $\xi_1(\vec{r}, t)$ in Eqs. (1) is a real Gaussian noise with intensity η_1, zero mean and δ-correlated in time and space, that accounts for local fluctuations in the external feeding μ.

2.2. Threshold analysis

We proceed to analyze the stability of the steady state solution under Poiseuille flow. Inspired by Ref. [47], we linearize Eqs. (1) around the uniform solution $a_1 = 1/\mu$ and $b_1 = \mu$, the eigenvalues $\omega(q_x)$ of the linear instability problem are obtained in terms of the wavevectors

$$\Delta a_1 = \tilde{a}(y)\exp(iq_x x + \omega t), \tag{3}$$
$$\Delta b_1 = \tilde{b}(y)\exp(iq_x x + \omega t), \tag{4}$$

through the following boundary eigenvalue problem

$$\begin{pmatrix} -\mu^2 & -2 \\ \mu^2 & 1 - q_x^2 - iq_x\phi(y) + \partial_{yy}^2 \end{pmatrix}\begin{pmatrix}\tilde{a}\\ \tilde{b}\end{pmatrix} = \omega\begin{pmatrix}\tilde{a}\\ \tilde{b}\end{pmatrix}. \tag{5}$$

This system was diagonalized numerically. In particular, a space discretization of the y-axis into N points was considered in order to get the eigenvalues ω. Note that by reflection symmetry around the x-axis, the original $2N \times 2N$ matrix (a square $N \times N$ matrix for each component) can be reduced to an $(N+1) \times (N+1)$ effective problem after an adequate discretization.

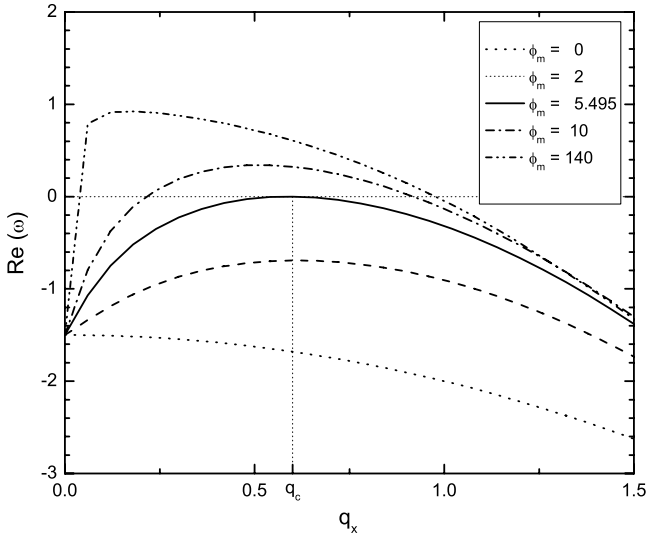

Fig. 1. Growth rate as a function of q_x for $\mu = 2$, for different values of the flux. The solid line corresponds to criticality and the critical wavevector q_c is also identified. The most unstable modes are associated with the maximum of each line. The level $\mathrm{Re}(\omega_c) = 0$ is also indicated as a dotted horizontal line as reference.

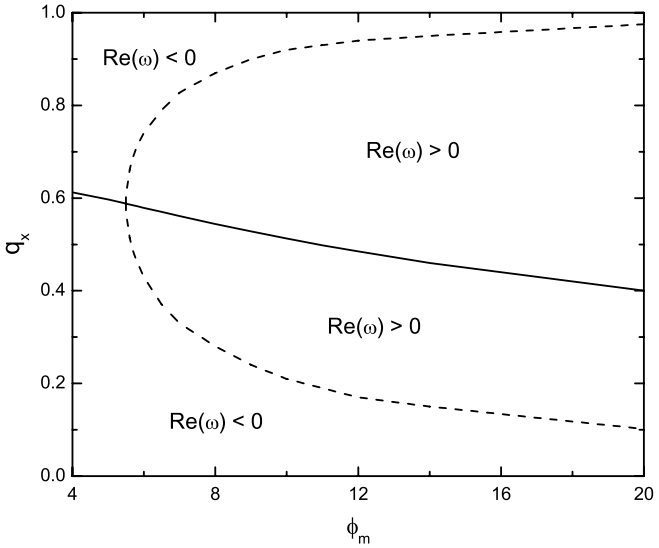

Fig. 2. Solid line: wavevector q_x of the most unstable mode as a function of ϕ_m for $\mu = 2$. Dashed line: boundaries for the band of unstable modes. The stability of each region (sign of the growth rate) is indicated.

The eigenvalues were numerically obtained for $N = 101$. In particular, we concentrate on the critical mode because it has the largest growth rate in the linear regime.

In Fig. 1 we show the growth rate of the critical mode a function of q_x. The curves correspond to different values of ϕ_m. Criticality [$\mathrm{Re}(\omega) = 0$] takes place at $q_x = q_c$ for $\phi_m = \phi_c$. For example, for $\mu = 2$ the critical values correspond to $\phi_c = 5.495 \pm 0.001$ at $q_c = 0.5882$.

For $\phi > \phi_c$ a band of unstable modes are expected, as we show in Fig. 1 for their corresponding growth rates. The dominant mode and the boundaries of the unstable mode bands are shown in Fig. 2, where the stability of each region is indicated.

2.3. Pattern formation

Numerical simulations above threshold confirm a finite wavelength instability and noise sustained structures are observed in this regime, as we illustrate in Fig. 3 for $\mu = 2$ and $\phi_m = 5.5$. Except explicit indication here after we take $L_y = 2L_x = 512$. Note that near threshold the time scale is very slow and long times are required to observe macroscopic structures. To avoid working with very large systems, periodic boundary conditions were considered in the x direction. In such a way the pattern formation results are accelerated. Nevertheless, long transients are also observed in this case near the critical flux.

By increasing ϕ_m a band of unstable modes are activated and well-developed macroscopic structures are observed in a reasonable timescale, as we show in Fig. 4 for $\phi_m = 10$. We remark that the patterns are not stationary but drift in

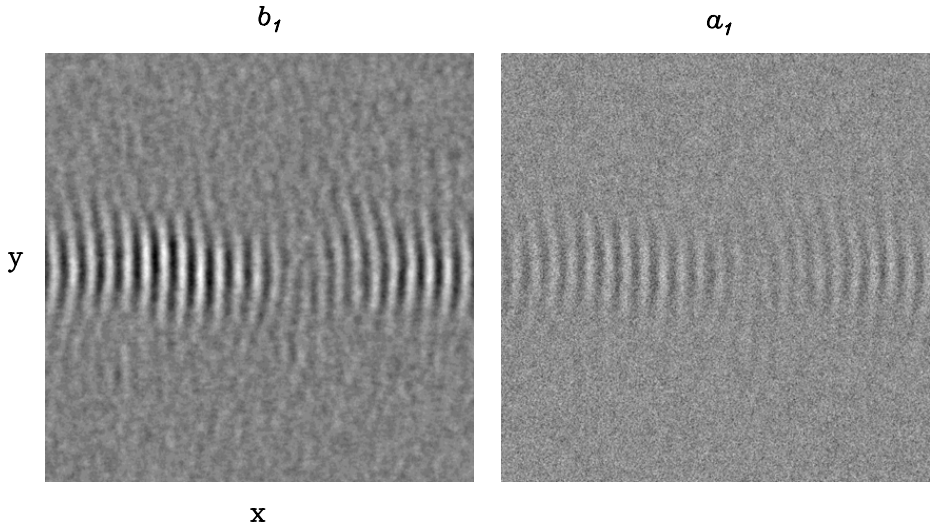

Fig. 3. Snapshot of b_1 and a_1 spontaneously generated from random initial conditions close to the steady state for $\mu = 2$. The system is near criticality and long times are required to observe patterns from finite-wavelength instabilities. Here $\phi_m = 5.5$ ($\phi_c = 5.495$), $t = 380\,000$ and $\eta_1 = 3 \times 10^{-5}$. We show only a central spot (256 × 200 grid points) where the self-organization can be appreciated.

the direction of the flow. Although the structures travel to the right, they are continuously regenerated by dynamical amplification of noise that excites all the unstable modes at each space point – locally sustained. At the left of the pattern the generation from noise of small-amplitude structures can be appreciated. This is a typical feature of NSS in two spatial dimensions [32,45]. In the same sense the resulting stripe pattern exhibits modulation of the fronts in the y direction produced by the external flow.

It is interesting to relate ϕ_c with the one corresponding to uniform flow ϕ_{th} (see Ref. [45] for analytical expression). We numerically observe that $(3/2)\phi_c > \phi_{th}$ but finally, as the flow decreases along the y-axis, the systems result locally stable far from the central axis. In consequence the resulting structure is expected to be localized around a centered band, as we illustrate in Fig. 4.

3. Synchronization of coupled systems

3.1. The model

Hereafter, system 1 is assumed to drive – in a master–slave configuration – another system (lying in a second differential-flow reactor) with the same values of μ and ϕ but with a possibly different noise intensity η_2

$$\partial_t a_2 = \mu - a_2 b_2^2 + \xi_2(\vec{r}, t),$$
$$\partial_t b_2 = \nabla^2 b_2 - \vec{\phi} \cdot \vec{\nabla} b_2 - b_2 + a_2 b_2^2 + \epsilon(b_1 - b_2). \tag{6}$$

Here ϵ denotes the strength of the unidirectional linear coupling between both reactors. As expected, the instability of the uniform solution $a_1 = a_2 = 1/\mu, b_1 = b_2 = \mu$ takes place at $\phi = \phi_c$, and it is driven by reactor 1 which remains uncoupled. Numerical simulations were performed of Eqs. (1) and (6) to characterize the synchronization of the resulting nonequilibrium extended structures of both reactors.

3.2. Synchronization

In Fig. 5 we show numerical results, in the presence of noise, for typical snapshots of b_1, a_1 (up) and b_2, a_2 (down) after ϕ_m is increased beyond its critical value. We can appreciate that reactors 1 and 2 support well-correlated NSS. To illustrate the correlation, in Fig. 6(a) and (b) we show the deviation fields α and β in the same scale of a_1, b_1, where

$$\alpha = a_1 - a_2,$$
$$\beta = b_1 - b_2. \tag{7}$$

The order of magnitude of α and β indicates an effective replication of the NSS in the first reactor takes place at the second one. The same phenomenon is also observed far from threshold as we illustrate in Fig. 7, where well developed and correlated NSS can be observed in the slaved reactor.

To quantify the phenomenon we introduce the global synchronization error $E(t)$, given by

$$E^2 = \frac{1}{L_x L_y} \int_A (\alpha^2 + \beta^2)\, \mathrm{d}x\, \mathrm{d}y, \tag{8}$$

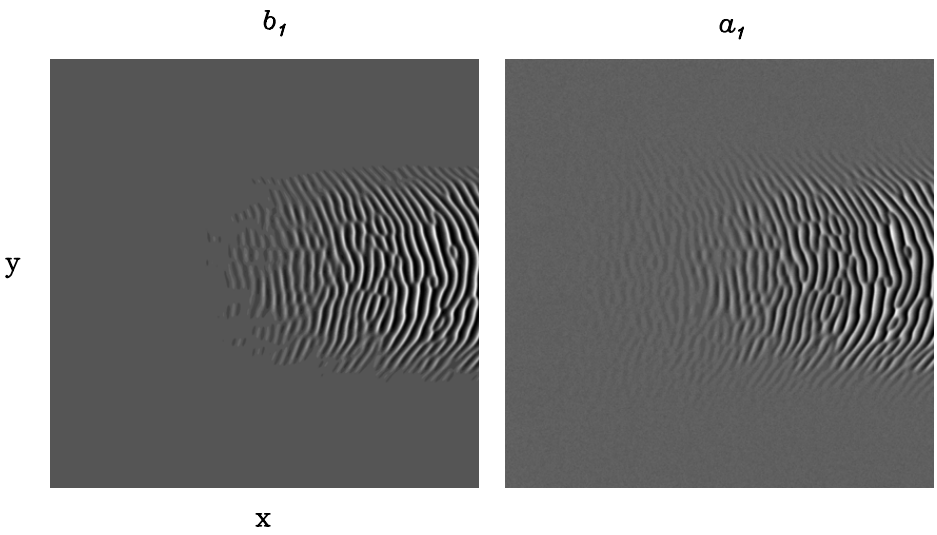

Fig. 4. Snapshot of a well developed NSS for a typical realization of Eq. (1). The whole structure of the patterns can be appreciated for a_1 and b_1, being the stripe patterns centered along the longitudinal axis of the reactor. A region with small modulations around the steady state can be appreciated at the left of each pattern, while two regions (up and down) remain below threshold (i.e., at the steady state) because the viscous boundary conditions. Parameters are $\mu = 2$, $\phi_m = 10$, $t = 160$ and $\eta_1 = 3 \times 10^{-5}$.

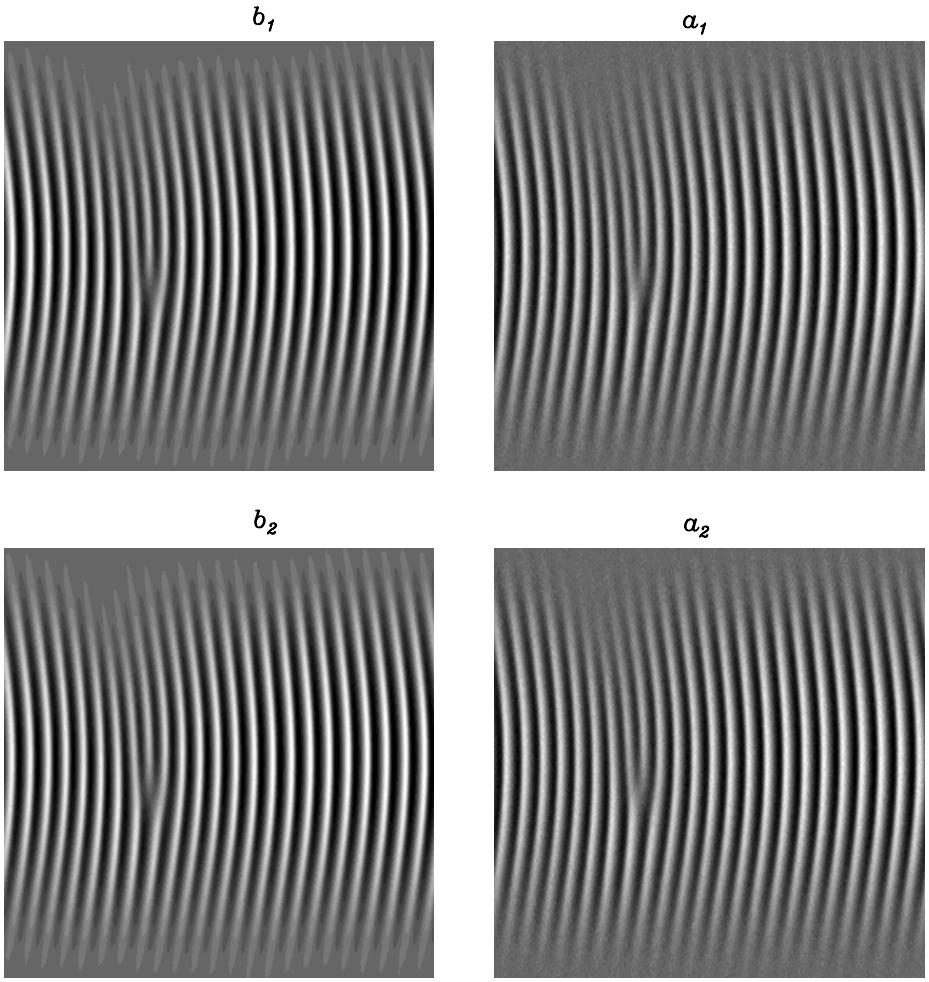

Fig. 5. Snapshots of synchronized NSS spontaneously generated from random initial conditions close to the trivial steady state. Up (down): macroscopic structures in reactor 1 (2). We show only a central spot (256×100 grid points) where the stripe pattern can be appreciated. Parameters are $\mu = 2.0$, $\phi_m = 6$, $\epsilon = 0.2$, $t = 320$ and $\eta_{1,2} = 3 \times 10^{-5}$.

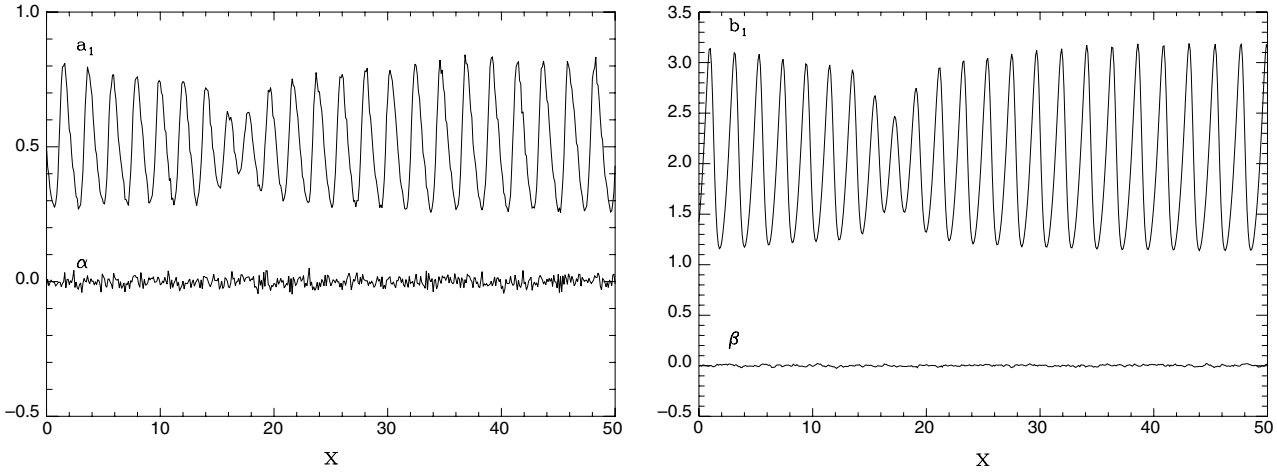

Fig. 6. (a) Detail of the pattern for a_1 and the corresponding deviation field α as results from a cut of the structures of Fig. 5 along $y = 0$. Both profiles are in the same scale. (b) The same for b_1 and β.

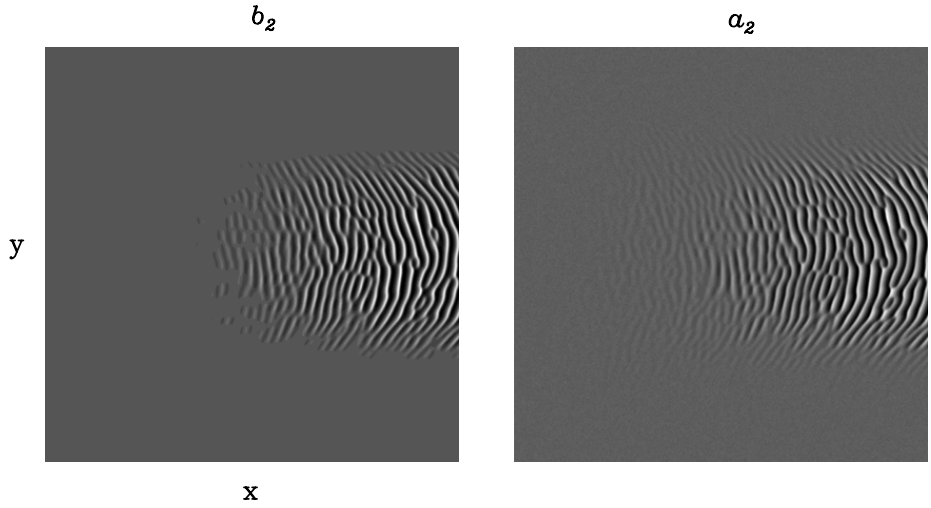

Fig. 7. Snapshots of a synchronized NSS in reactor 2 corresponding to the one showed in Fig. 4 for reactor 1. Here $\epsilon = 0.2$ and $\eta_2 = \eta_1$.

and two one-component estimators, the respective α and β-variances

$$\sigma_\alpha^2 = \frac{1}{L_x L_y}\int_A (\langle\alpha^2\rangle - \langle\alpha\rangle^2)\,\mathrm{d}x\,\mathrm{d}y$$
$$\sigma_\beta^2 = \frac{1}{L_x L_y}\int_A (\langle\beta^2\rangle - \langle\beta\rangle^2)\,\mathrm{d}x\,\mathrm{d}y, \tag{9}$$

where A means integration extended over all values of L_x and L_y (the whole reactor).

The time evolution of the sync-estimators can be observed in Fig. 8 for a typical realization of Eqs. (1) and (6). After a transient, the three estimators reach a plateau when the synchronized structures are well developed. Note that $E(t)$, which basically accumulates information of both variances, results given essentially by σ_β.

A dependence of E on control parameters ϵ and ϕ_m is expected, as far as ϕ_m measures distance to the critical point while ϵ denotes the strength of the linear coupling. In Fig. 9 we show E *vs.* ϵ after the transient regime. Here the bars indicate the dispersion for averages over 20 realizations. Clearly the sync's magnitude (value of E) and the sync's quality (value of E-dispersion) decrease with ϵ. Similarly, in Fig. 10 we show E as a function of ϕ_m. As expected, the magnitude of the sync decreases far from threshold, where an increasing number of unstable modes are active. A linear dependence of E with ϕ_m is numerically observed near threshold.

Numerical simulations (not shown) indicate that local replication of NSS can also be obtained if only finite regions of the reactors are coupled. For example, if a nonuniform spatial coupling is considered where $\epsilon \neq 0$ only in a finite longitudinal band centered along the axis x, local replication is observed exclusively inside that band.

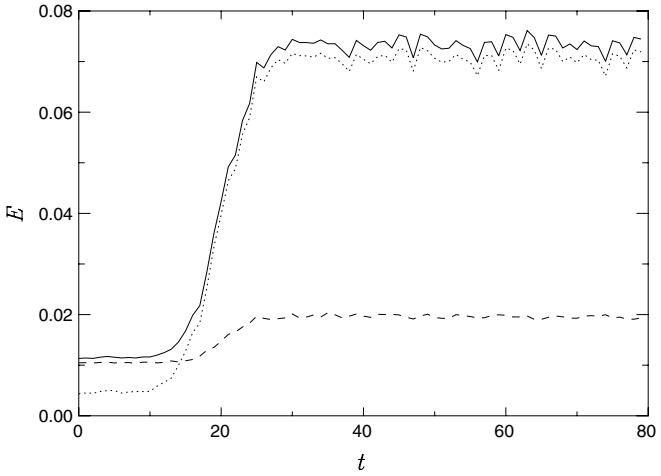

Fig. 8. Time evolution of the global synchronization error E (solid line) for a typical realization of Eqs. (1) and (6). In dotted (dashed) line we also show the β (α) variances. Parameters are $\phi_m = 10$, $\epsilon = 0.3$ and $\eta_{1,2} = 3 \times 10^{-5}$.

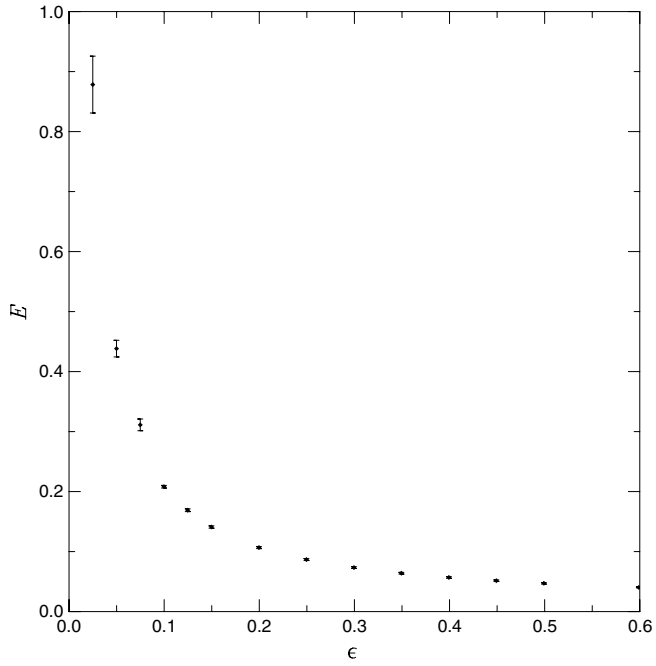

Fig. 9. Averaged global synchronization error E (and dispersions), as a function of ϵ for constant flux $\phi_m = 10$ after the transient regime. Parameters are $\mu = 2$ and $\eta_{1,2} = 3 \times 10^{-5}$.

3.3. Stability of the synchronized manifold

Since the drive and the response systems synchronize, we expect the manifolds $a_1 = a_2$ and $b_1 = b_2$ to be at least linearly stable. This is however difficult to prove analytically from the linearized equations for α and β, due to the noise-sustained nature of the "unperturbed" patterns $(a_1(x, y, t), b_1(x, y, t))$ and the nonuniformities of the flow. An approach to the stability of the synchronization manifold flux was presented in Ref. [34] for uniform flow and it is extended here for Poiseuille flow.

The linear stability analysis for (α, β) around the uniform rest state confirms that the synchronization manifolds are linearly stable above ϕ_c. However, the numerical observation also suggests the stability in the nonlinear regime, where the structures are well developed. An approach to the problem consist in getting information about the asymptotic behavior of the synchronized manifold. From Eqs. (1) and (6) we see that the full, nonlinear evolution equation for β can be cast in the form

$$\partial_t \beta = \hat{L}\beta + J(x, y, t), \tag{10}$$

with

$$\hat{L} = \nabla^2 - \phi(y)\partial_x - (1 + \epsilon), \tag{11}$$

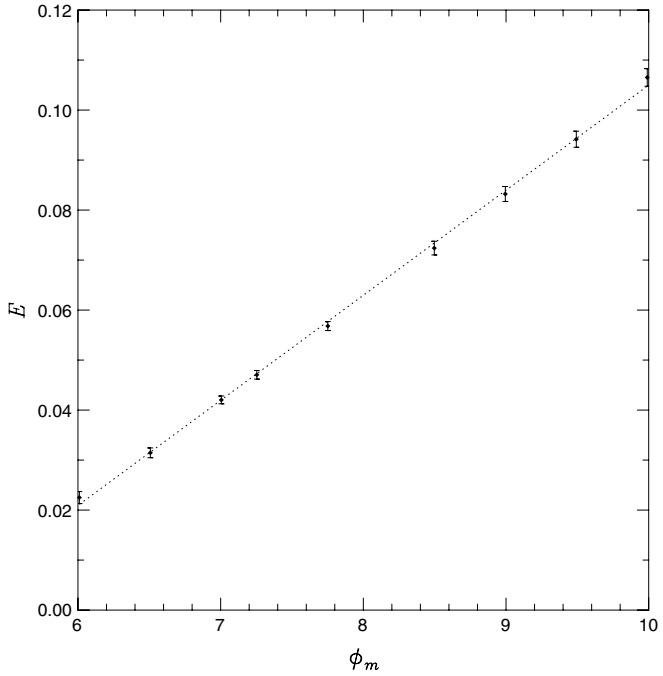

Fig. 10. Averaged global synchronization error (and dispersions) as a function of ϕ_m for constant spatial coupling ($\epsilon = 0.2$) after the transient regime. In solid line we show a linear fit by minimum squares. Parameters are $\mu = 2$ and $\eta_{1,2} = 3 \times 10^{-5}$.

and we have introduced a "noisy source"

$$J = a_1\, b_1^2 - a_2\, b_2^2, \tag{12}$$

whose convolution with the Green function of $\hat{L}$ formally determines the time evolution and the asymptotic behavior of β. Similarly we can obtain an evolution equation for α. However, for convenience we introduce a new variable $\gamma = \alpha + \beta$. The full evolution equation for γ reads

$$\partial_t \gamma = \hat{L}\beta. \tag{13}$$

The numerical characterization of J above threshold (i.e., the nonlinear regime) indicates a zero mean source with finite variances which depend on the parameters, as expected. For example, in Fig. 11 we show the J-variance σ_J (reactor's average) as a function of ϵ. The same for σ_J *vs.* ϕ_m in Fig. 12. In both figures $|\langle J\rangle|$ remains below $10^{-3}\sigma_J$. For example in Fig. 12, $|\langle J\rangle|/\sigma_J$ equals 10^{-3} at $\phi_m = 6$ and 4×10^{-4} at $\phi_m = 12$. A trivial monotonically increasing dependence of variances with the noise intensities is numerically observed, as expected if we consider that both reactors are driven by independent sources of noise.

To characterize the asymptotic dynamics of Eq. (10) we proceed to introduce the Fourier amplitudes $\tilde{\beta}(y)$ along the x-axis

$$\beta = \tilde{\beta}(y)\exp(iq_x x + \omega t), \tag{14}$$

that leads the following boundary eigenvalue problem

$$[\mathrm{d}^2/\mathrm{d}y^2 - q_x^2 - iq_x\phi(y) - (1+\epsilon)]\,\tilde{\beta} = \omega\,\tilde{\beta}, \tag{15}$$

that we solve numerically. In Fig. 13 we show $\mathrm{Re}(\omega)$ as a function of q_x for the least stable mode. From its behavior we conclude that the full spectrum is dissipative [$\mathrm{Re}(\omega_i) < 0$] and remains far from any instability point. By inspection we see that the least stable mode corresponds to $q_x = 0$. In this case Eq. (15) simplify considerably and we get the analytical result $\omega(0) = -(1+\epsilon)$.

The main point is that the linear operator $\hat{L}$ has a strongly dissipative character. When the convolution of the well-behaved and bounded source J with the Green function of $\hat{L}$ is taken into account, damped dynamics results for β as a consequence. This can be observed, for example, through the spectral representation of G, where the eigenvalues appear explicitly.

Once the β stability is granted, Eq. (13) determines the stability of γ and therefore the stability of the synchronized manifold.

4. Conclusions

We have investigated the role of an external flow with viscous boundary conditions in the context of pattern-formation and synchronization of macroscopic structures for cubic stochastic kinetics developing in extended chemical reactors.

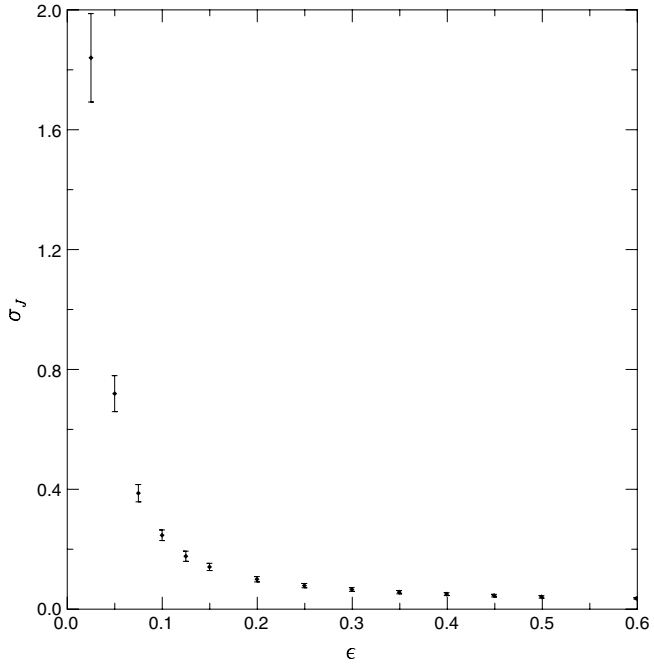

Fig. 11. σ_J *vs.* ϵ. Parameters as in Fig. 9.

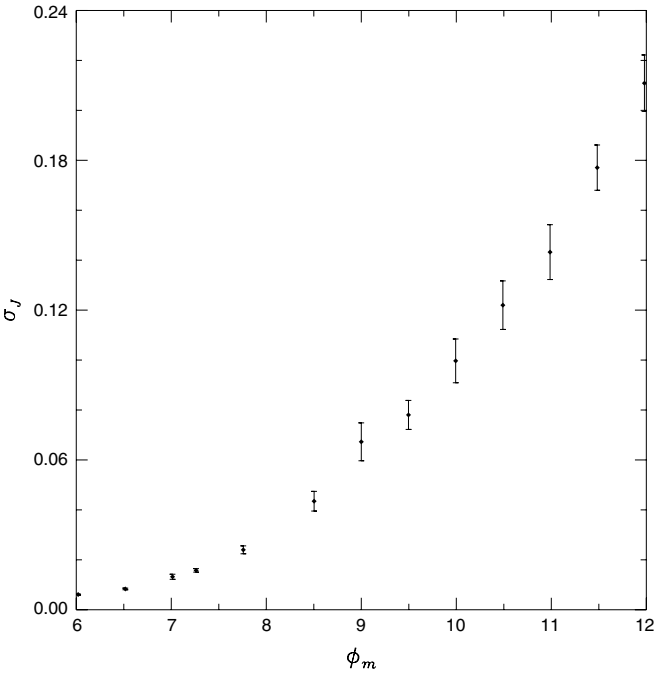

Fig. 12. σ_J *vs.* ϕ_m. Parameters as in Fig. 10.

Particularly, for a Gray–Scott kinetics evolving in packed-bed reactors under Poiseuille flows we have characterized a finite-wavelength instability induced by the flow. Thresholds and growth rates of the unstable modes were elucidated and numerical simulations confirm the expected instability and the related formation of macroscopic noise-sustained structures. They appear spontaneously in both activator and inhibitor species when the advection is above the critical value. These structures are the result of selective noise amplification by the dynamics in several orders of magnitude leading to the formation of stochastic self-organized structures. Special features appear, due to nature of the external flow. In particular, it induces curved-stripe patterns that "follow" the velocity-flow profile. In consequence, the patterns result localized: only the central region of reactor remains "activated" (i.e., above threshold) producing the observed structures, while the reactives remain at the steady state near the reactor's longitudinal boundaries. In this way, regions of uniform steady state coexist with macroscopic structures along the reactor. Note that the stability of the reactor is reinforced under Poiseuille flow. On one hand, the instability threshold increases with respect to that of uniform flow. On the other hand, modulational instabilities

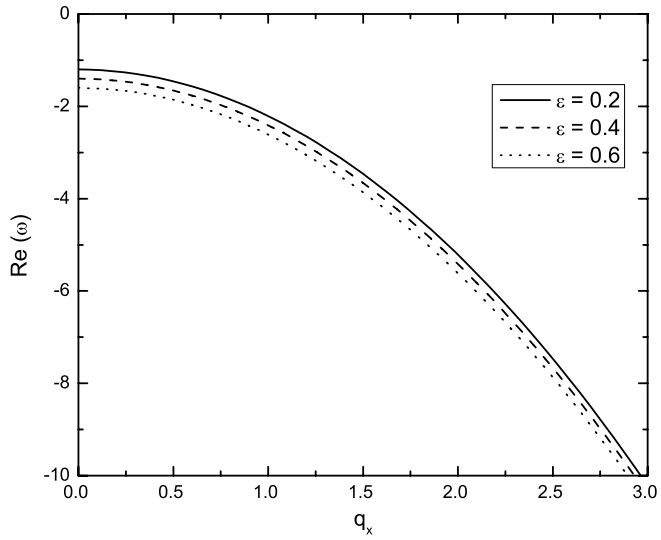

Fig. 13. Growth rates of the least stable Fourier modes of Eq. (15) as a function of q_x. The curves correspond to $\phi_m = 10$, and different values of spatial coupling. For the flux values considered in this work the curves are similar and the difference cannot be appreciated in the figure's scale.

and fragmentations of the fronts are not observed for realistic values of the flux. As a consequence, both regimes become more stable against external fluctuations.

For the same kinetics and constraints, but coupling unidirectionally the corresponding points of two differential-flow reactors, we have characterized the synchronization between NSS. We have observed that the usual estimators of synchrony – like correlators or global synchronization error – indicate a replication of macroscopic convective structures for appropriate values of the strength coupling. We have also shown that the correlation is present point to point and this means that the phenomenon is spatially distributed. We numerically observe the robustness of the phenomenon under changes in parameters above threshold. In particular, synchronization increases (decreases) with the strength of coupling (external flow).

From the theoretical point of view, we have characterized the stability of the synchronized manifolds in terms of an effective dynamics of damped Fourier modes. Analytical results for the sync-manifolds' stability are only available around the uniform solutions. However, we have shown that the main scenario of synchronization related with damped dynamics of the deviation field's Fourier modes remain valid even around stochastic macroscopic structures.

We point out that chemical NSS should be observable for different chemical reactions in differential-flow reactors. The imposed flow breaks the spatial symmetry of the system for any reaction in a generic way, allowing eventual convective instabilities. Thus, we expect chemical NSS to be observed in differential-flow reactors under very general conditions. To conclude, we observe that the synchronization is robust under changes in coupling and flows, and we expect this to have technological applications in the control of differential-flow reactors. Note that the local or global replication of chemical structures through synchronization appears as a possible technological way to manipulate macroscopic structures. In this sense, we expect that our results can be extended to more general convectively unstable reactions/reactors.

Acknowledgments

We acknowledge financial support from CONICET (Argentina), through Project PIP R2201009003/5, and Universidad Nacional de Mar del Plata (UNMdP, Argentina) through Projects EXA505/10 and EXA544/11.

References

[1] C. Huygens, Sur la sympathie des horloges, J. des Sçavants 11 (1665) 79–80.
[2] C. Huygens, Sur la sympathie des horloges, J. des Sçavants 12 (1665) 86.
[3] A.T. Winfree, The Geometry of Biological Time, Springer, New York, 1980.
[4] A. Pikovsky, M. Rosenblum, J. Kurths, Synchronization: A Universal Concept in Nonlinear Science, CUP, Cambridge, 2001.
[5] S.H. Strogatz, Sync: The Emerging Science of Spontaneous Order, Penguin, New York, 2004.
[6] J.A. Acebrón, L.L. Bonilla, C.J.P. Vicente, F. Ritort, R. Spigler, The Kuramoto model: a simple paradigm for synchronization phenomena, Rev. Modern Phys. 77 (2005) 137–185.
[7] A. Arenas, A. Díaz-Guilera, J. Kurths, Y. Moreno, C. Zhou, Synchronization in complex networks, Phys. Rep. 469 (2008) 93–153.
[8] A. Balanov, N. Janson, D. Postnov, O. Sosnovtseva, Synchronization: From Simple to Complex, Springer, Berlin, 2008.
[9] A. Stefanski, Determining Thresholds of Complete Synchronization, and Application, World Scientific, Singapore, 2009.
[10] C. Zhou, J. Kurths, Dynamical weights and enhanced synchronization in adaptive complex networks, Phys. Rev. Lett. 96 (2006) 164102.
[11] C. Zhou, A. Motter, J. Kurths, Universality in the synchronization of weighted random networks, Phys. Rev. Lett. 96 (2006) 034101.
[12] P. Donetti, P. Hurtado, M. Muñoz, Entangled networks, synchronization, and optimal network topology, Phys. Rev. Lett. 95 (2005) 188701.
[13] A.T. Winfree, Biological rhythms and the behavior of populations of coupled oscillators, J. Biol. Chem. 16 (1967) 15–42.

[14] Y. Kuramoto, in: H. Araki (Ed.), Proceedings of the International Symposium on Mathematical Problems in Theoretical Physics, in: Lecture Notes in Physics, vol. 39, Springer, Berlin, 1975.
[15] Y. Kuramoto, Chemical Oscillations, Waves, and Turbulence, Springer, Berlin, 1984.
[16] L.M. Pecora, T.L. Carroll, Synchronization in chaotic systems, Phys. Rev. Lett. 64 (1990) 821–824.
[17] M.G. Rosenblum, A.S. Pikovsky, J. Kurths, Phase synchronization of chaotic oscillators, Phys. Rev. Lett. 76 (1996) 1804–1807.
[18] N.F. Rulkov, M.M. Sushchik, T.S. Tsimring, H.D.I. Abarbanel, Generalized synchronization of chaos in directionally coupled chaotic systems, Phys. Rev. E 51 (1995) 980–994.
[19] L. Kocarev, U. Parlitz, Generalized synchronization, predictability, and equivalence of unidirectionally coupled dynamical systems, Phys. Rev. Lett. 76 (1996) 1816–1819.
[20] C. Serrat, M. Torrent, J. García-Ojalvo, R. Vilaseca, Synchronization-induced noise reduction in spatially coupled microchip lasers, Phys. Rev. A 64 (2001) 041802(R).
[21] P. Parmananda, Generalized synchronization of spatiotemporal chemical chaos, Phys. Rev. E 56 (1997) 1595–1598.
[22] L. Kocarev, Z. Tasev, U. Parlitz, Synchronizing spatiotemporal chaos of partial differential equations, Phys. Rev. Lett. 79 (1997) 51–54.
[23] L. Junge, U. Parlitz, Synchronization and control of coupled Ginzburg–Landau equations using local coupling, Phys. Rev. E 61 (2000) 3736–3742.
[24] S. Boccaletti, J. Bragard, F.T. Arecchi, H. Mancini, Synchronization in nonidentical extended systems, Phys. Rev. Lett. 83 (1999) 536–539.
[25] H. Chaté, Spatiotemporal intermittency regimes of the one-dimensional complex Ginzburg–Landau equation, Nonlinearity 7 (1994) 185.
[26] A. Amengual, E. Hernández-García, R. Montagne, M. San Miguel, Synchronization of spatiotemporal chaos: the regime of coupled spatiotemporal intermittency, Phys. Rev. Lett. 78 (1997) 4379–4382.
[27] E. Hernández-García, M. Hoyuelos, P. Colet, M. San Miguel, R. Montagne, Spatiotemporal chaos, localized structures and synchronization in the vector complex Ginzburg–Landau equation, Internat. J. Bifur. Chaos 9 (1999) 2257.
[28] E. Hernández-García, M. Hoyuelos, P. Colet, M. San Miguel, Dynamics of localized structures in vectorial waves, Phys. Rev. Lett. 85 (2000) 744.
[29] M.A. Muñoz, R. Pastor-Satorras, Stochastic theory of synchronization transitions in extended systems, Phys. Rev. Lett. 90 (2003) 204101.
[30] S. Hod, Analytic treatment of the network synchronization problem with time delays, Phys. Rev. Lett. 105 (2010) 208701.
[31] D. Hunt, G. Korniss, B.K. Szymanski, Network synchronization in a noisy environment with time delays: fundamental limits and trade-offs, Phys. Rev. Lett. 105 (2010) 068701.
[32] G. Izús, M. Santagiustina, M. San Miguel, P. Colet, Pattern formation in the presence of walk-off for a type II optical parametric oscillator, J. Opt. Soc. Amer. B 16 (1999) 1592–1596.
[33] G. Izús, P. Colet, M. San Miguel, M. Santagiustina, Synchronization of vectorial noise-sustained structures, Phys. Rev. E 68 (2003) 036201.
[34] G.G. Izús, R.R. Deza, A.D. Sánchez, Replication of noise-sustained autocatalytic chemical structures, J. Chem. Phys. 132 (2010) 234112.
[35] R. Deissler, Noise-sustained structure, intermittency, and the Ginzburg–Landau equation, J. Stat. Phys. 40 (1985) 371–395.
[36] R. Deissler, External noise and the origin and dynamics of structure in convectively unstable systems, J. Stat. Phys. 54 (1989) 1459–1488.
[37] W. van Saarloos, P.C. Hohenberg, Fronts, pulses, sources and sinks in generalized complex Ginzburg–Landau equations, Physica D 56 (1992) 303.
[38] M.A. Scherer, G. Ahlers, Temporal and spatial properties of fluctuations below a supercritical primary bifurcation to traveling oblique-roll electroconvection, Phys. Rev. E 65 (2002) 051101.
[39] K.L. Babcock, G. Ahlers, D.S. Cannell, Noise-sustained structure in Taylor–Couette flow with through flow, Phys. Rev. Lett. 67 (1991) 3388–3391.
[40] A. Tsameret, V. Steinberg, Noise-modulated propagating pattern in a convectively unstable system, Phys. Rev. Lett. 67 (1991) 3392–3395.
[41] E. Louvergneaux, C. Szwaj, G. Agez, P. Glorieux, M. Taki, Experimental evidence of absolute and convective instabilities in optics, Phys. Rev. Lett. 92 (2004) 043901.
[42] M. Santagiustina, P. Colet, M. San Miguel, D. Walgraef, Two-dimensional noise-sustained structures in optical parametric oscillators, Phys. Rev. E 58 (1998) 3843–3853.
[43] M. Santagiustina, P. Colet, M. San Miguel, D. Walgraef, Noise-sustained convective structures in nonlinear optics, Phys. Rev. Lett. 79 (1997) 3633–3636.
[44] M. Santagiustina, P. Colet, M. San Miguel, D. Walgraef, Growth dynamics of noise-sustained structures in nonlinear optical resonators, Opt. Express 3 (1998) 63–70.
[45] B. von Haeften, G. Izús, Noise-sustained structures in differential-flow reactors with autocatalytic kinetics, Phys. Rev. E 67 (2003) 056207.
[46] G.G. Izús, R.R. Deza, L.J. Bernal, V. Pérez-Villar, Complete synchronization of convective patterns between Gray–Scott systems, Eur. Phys. J. Special Topics 143 (2007) 135–141.
[47] D.A. Vasquez, Chemical instability induced by a shear flow, Phys. Rev. Lett. 93 (2004) 104501.